Applied Geochemistry 64 (2016) 10–21

Contents lists available at ScienceDirect

Applied Geochemistry

journal homepage: www.elsevier.com/locate/apgeochem

Arsenic and lead mobility: From tailing materials to the aqueous compartment

Alexandra Courtin-Nomade [a, *], Thomas Waltzing [b], Catherine Evrard [a], Marilyne Soubrand [a], Jean-François Lenain [a], Emmanuelle Ducloux [a], Sonda Ghorbel [a], Cécile Grosbois [c], Hubert Bril [a]

[a] Université de Limoges, GRESE, E.A. 4330, 123 Avenue A. Thomas, 87060 Limoges Cedex, France
[b] KONIAMBO NICKEL SAS, Route Territoriale 1, Site de Vavouto – 98833 Voh, BP 679–98860 Koné, New Caledonia
[c] Université François Rabelais de Tours, EA 6293 GéHCO, Parc de Grandmont, 37200 Tours, France

ARTICLE INFO

Article history:
Received 1 June 2015
Received in revised form
18 September 2015
Accepted 21 September 2015
Available online 7 November 2015

Keywords:
Tailings
Lead
Arsenic
Mineralogy
Leaching tests

ABSTRACT

This study concerns the mineralogy of the tailings of a former Ag–Pb mine (Auzelles district, France) and the contribution of the waste materials to the heavy metal dissemination in the environment. Accumulation of metals in fish flesh was reported and this pollution is attributed to past mining activities. Tailings were studied to establish the major transfer schemes of As and Pb in order to understand their mobility that leads to contamination of a whole ecosystem. Mineralogical investigation, solubility and compliance tests were performed to assess the stability of the metal-bearing phases. Among the various metallic elements measured, As and Pb show the highest bulk concentrations (up to 0.7% and 6.3% respectively) especially for samples presenting near neutral pH values. According to X-ray diffraction (XRD), Scanning Electron Microscopy (SEM-EDX), Electron Probe Micro-Analysis (EPMA) and micro-Raman spectrometry (μRS), tailings mineralogy still contain primary minerals such as sulfides (*e.g.,* galena, pyrite), phosphates (monazite, apatite) and/or carbonates (*e.g.,* (hydro-)cerussite, dolomite, siderite). Sulfates (*e.g.,* anglesite, lanarkite, plumbojarosite and beudantite) are the main secondary metal-bearing phases with other interesting phases accounting for metals mobility such as Fe and/or Pb and/or Mn oxides (*e.g.,* lepidocrocite, goethite -up to 15 wt% of Pb was measured-, plumboferrite-type phase, mimetite). The lowest Pb solubilities were obtained at pH 8–9 and at a larger range than for As for which the lowest solubilities are reached around pH 6–7. At this minimum solubility pH value, Pb concentrations released still over exceed the National Environmental Quality Standards (NEQS), whatever the samples. The highest solubility is reached at pH 2 for both elements whatever the considered sample. This represents up to 51% of total Pb and up to 46% of total As remobilized and concentrations exceeding the NEQS. As and Pb released mainly depends on the Fe/Mn oxides (*e.g.,* goethite, lepidocrocite) and carbonates (cerussite) which are the less stable phases. Compliance tests also show that Pb concentrations released are higher than the upper limit for hazardous waste landfills. Determination of the mineralogy allows understanding both the solubility and leaching test experiments results, as well as to forecast the impact of the residues on the water quality at a mid-term scale.

1. Introduction

Numerous waste dumps and tailings are common leftover of former mining activities all over the world and the French Massif Central in France is no exception. This region was one of the highest polymetallic producers in Europe until the mid-20th century. These activities led to contamination of soils, sediments, biota and alter water quality of the rivers at various scales (see examples for this area, *e.g.,* Bossy et al., 2010; Courtin-Nomade et al., 2012, 2010, 2003; Grosbois et al., 2012, 2009, 2007; Pascaud et al., 2013). Numerous studies have demonstrated the high toxicity of As and Pb in aqueous medium (water column and sediment) at all trophic levels: microorganisms, fish and algae (*e.g.,* Macdonald et al., 2000; Moriarty et al., 2014; Shuhaimi-Othman et al., 2012; Wetzel et al.,

* Corresponding author.
E-mail address: alexandra.courtin@unilim.fr (A. Courtin-Nomade).

http://dx.doi.org/10.1016/j.apgeochem.2015.11.002
0883-2927/

2013). Mineralogy of As and Pb host phases in mining environments has been also extensively studied (Courtin-Nomade et al., 2003; Donahue and Hendry, 2003; González-Corrochano et al., 2014; Hayes et al., 2012; Savage et al., 2000; Smuda et al., 2007; Yang et al., 2009) showing the importance of sulfates and Fe/Mn oxides in their sequestration. Depending on the mineralized vein paragenesis and the local lithology, Pb is identified as anglesite, the most frequent sulfate, plumbojarosite or beudantite (Arenas-Lago et al., 2014; Frau et al., 2009; Murray et al., 2014; Néel et al., 2003; Romero et al., 2010; Roussel et al., 2000) and its affinity with Fe and Mn compounds have been also highlighted (Courtin-Nomade et al., 2009; Miler and Gosar, 2012; Sejkora et al., 2012). Arsenic can be naturally attenuated in mining environments when associated to jarosite, iron oxides or present as scorodite or pharmacosiderite (Asta et al., 2009; Bossy et al., 2010; Craw et al., 2002; Drahota et al., 2009; Gault et al., 2005; Kocourková et al., 2011; Lee et al., 2005).

This study concerns a watershed affected by former Ag–Pb extraction belonging to the Auzelles district in the French Massif Central, and where only no-kill fishing practice is allowed (local French regulation) because of too high metal contents in fish flesh according to European limits. Results presented here concern tailings samples, characterized by complementary techniques (X-ray Diffraction, Scanning Electron Microscope (SEM), Electron Probe Micro-Analysis (EPMA) and micro-Raman spectroscopy (μ-RS)) and for which stability of metal host phases was assessed using various leaching experiments.

This study is the first one concerning the Ag–Pb Auzelles district and thus aims: (i) to characterize the mineralogy of the tailings, and especially to identify the As and Pb host phases; (ii) to determine the evolution with time of these host-phases (*e.g.,* weathering susceptibility, remobilization of As and Pb, impact on the water quality, natural attenuation) and establish the major transfer schemes of the metallic elements from the tailings in order to understand their mobility that leads to the contamination of the aqueous compartment.

2. Materials and methods

2.1. Site and materials description

The Auzelles district is located in the southeastern part of the French Massif central. The lithology of this area corresponds to migmatites with intrusive granite. The Miodet River (30 km long) crossed through this district and is a sub-tributary of the Loire River by the Dore River then by the Allier River (Fig. 1). The Miodet basin has a total surface area of approximately 100 km^2. Around 6t of Ag and 6000t of Pb were extracted from the district of Auzelles until the last 19th century (http://www.sigminesfrance.brgm.fr) to be treated in the Pontgibaud fundery located several thousand kilometers away on the western part of Clermont-Ferrand (Fig. 1). The activities began in 1869 and ceased in 1901 even if exploration operations occurred until 1960 (http://www.sigminesfrance.brgm.fr). The main mineralization consists of galena (PbS) and the accessory mineralization consists of sphalerite (ZnS), chalcopyrite (CuFeS), pyrite (FeS_2), arsenopyrite (FeAsS) and cerussite ($PbCO_3$) in a gangue of granite, quartz and clays, barite and carbonates (dolomite $CaMg(CO_3)_2$, calcite $CaCO_3$, siderite $FeCO_3$, ankerite $Ca(Fe,Mg,Mn)(CO_3)_2$) (http://www.sigminesfrance.brgm.fr).

These previous mining activities generated large volume of waste, estimated here to represent 100 000 m^3. These residues are treatment residues from physical–chemical processes (crushing and flotation) and are deposited on a slope overhanging the Miodet River (Fig. 1). They constitute large heaps of more or less coarse sandy material affected by retrogressive erosion due to meteoric water runoffs and present scarce vegetation if any. Thus erosional processes led to solid transport by runoff waters, wind and gravity toward this river. Tailings particles could directly fed the sediments affecting their quality. Alteration processes may also occur, leading to remobilization of heavy metals by oxidation and hydrolysis.

Furthermore the waste dumps are located 21.7 km away from a dam reservoir constituting a favorable settling system that may accumulate heavy metals. A prefectural decree was established in March 2010 prohibiting consumption of fishes caught all along the Miodet River. Indeed, Pb and Cd were measured within the trout fished near the tailings and downstream, exceeding the European consumption regulation (CE n°1881/2006) set at 0.3 and 0.05 mg/kg respectively (http://www.puy-de-dome.gouv.fr).

Twenty-seven samples of tailings have been collected with a plastic scoop on the heap according to the following criteria: texture, grain size, color and location. They have been air dried at room temperature and then sieved at <2 mm with Teflon mesh to remove any vegetation debris. Part of this fraction was used to prepare 30 μm thick thin sections using epoxy resin polymerized at low temperature (<40 °C) and another part was crushed with an agate mortar for X-ray diffraction, chemical analysis, solubility and leaching experiments.

2.2. Analytical techniques

2.2.1. Chemical parameters and characterization

The pH values of the waste materials were determined according to the normalized protocol NF ISO 10390. Chemical compositions were obtained by ICP-MS or ES (Inductively Coupled Plasma-Mass Spectrometry or Emission Spectrometry, ACME, certified laboratory, Can) following a Lithium metaborate/tetraborate fusion and nitric acid digestion. An aqua regia digestion was also performed for the precious and base metals. Some chemical analyses were also done by AAS-GF and AAS-F (Atomic Adsorption Spectrometer-Graphite Furnace or Flame, GRESE, Fr) after a four acid digestion using HNO_3, $HF + HClO_4$ and HCl using a hot plate. All measurements were performed on duplicates and some measurements were triplicate randomly. Reference materials were also used for quality control (STD SO-18 ACME standard). Analytical error was within 1% for major elements and within 10% for trace elements.

2.2.2. Solid characterization

The grain size distribution has been determined by the INRA certified laboratory (Laboratoire d'Analyses des Sols d'Arras, Fr) using five grain size classes according to the normalized protocol NF × 31–107. X-ray diffraction (XRD) was performed using a BRUKER D8 advance diffractometer (SPCTS, Limoges, Fr) and obtained from 2 to 80°2Θ with a step size of 0.02°and an acquisition time of 2s/step using $CuK_{\alpha 1,2}$ ($\lambda = 1.5418$ Å) radiation. Indexation was obtained with the EVA software and ICDD database.

Secondary (SE) and backscattered electron (BSE) images were obtained with a Philips XL30 scanning electron microscope (SEM) equipped with an EDX system (electron dispersive spectrometer X-ray analyzer) (SERMIEL, SPCTS, Limoges, Fr). The accelerating voltage was fixed at 20 kV and samples were coated with carbon prior analysis.

Micro-Raman spectroscopy (μRS) analyses were performed using a Jobin Yvon 6400 Raman spectrometer (SPCTS, Limoges, FR), combined with a 100× objective, which results in a spatial resolution of one micron. The excitation source is an Ar^+ laser (Coherent Radiation or Spectra Physics) operating at 514.5 nm. The incident power was limited to 2–5 mW with additional filters (D1 or D2). More experimental details on this setup have already been described in Courtin-Nomade et al. (2010).

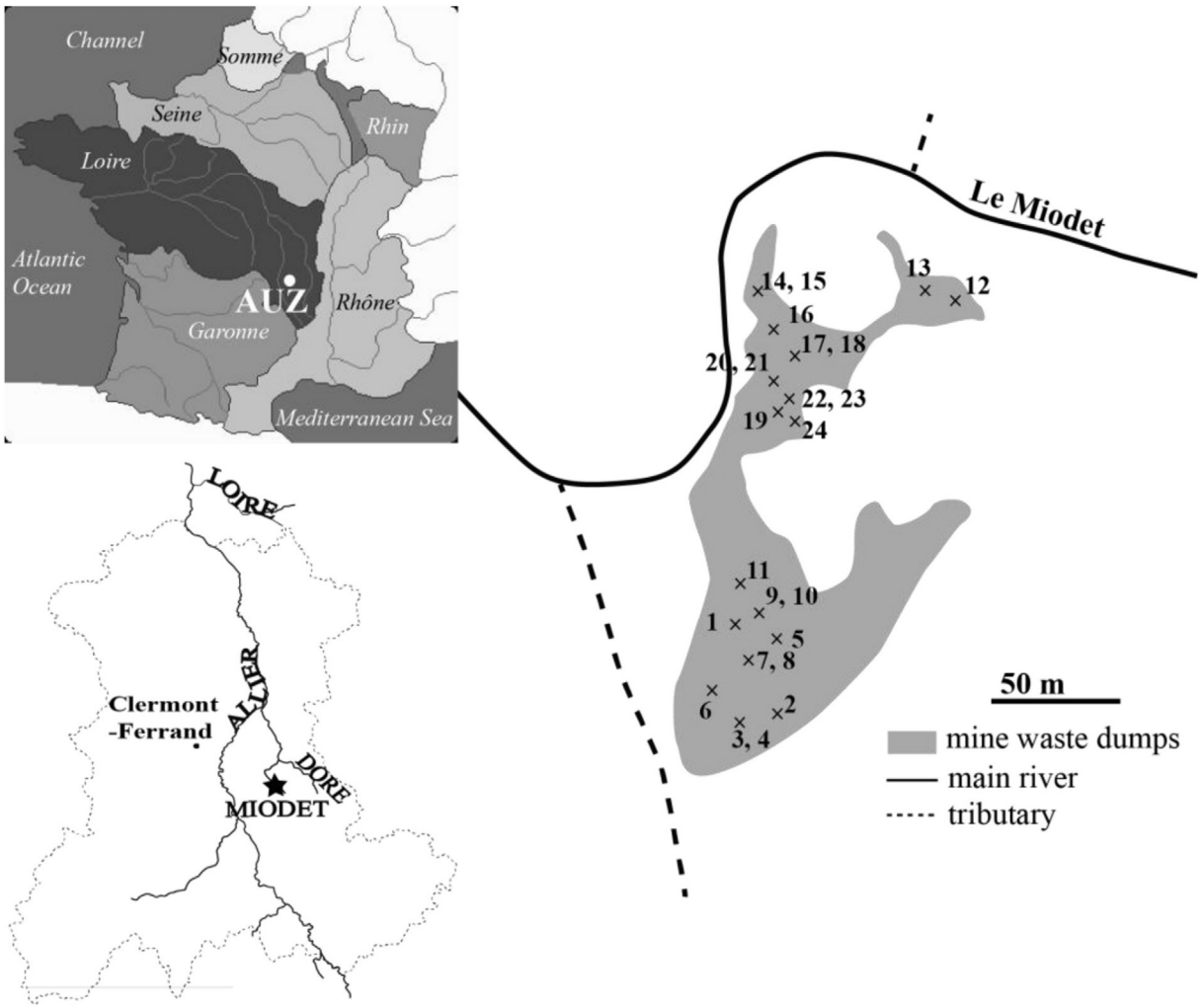

Fig. 1. Location of the Auzelles district at the scale of the Loire River basin and spatial configuration of the tailings and the local River (sample free areas are covered by vegetation). The star in the bottom left map indicates the location of the waste mine.

2.2.3. EPMA

BSE imaging and quantitative analysis were obtained with a Cameca SX100 electron microprobe at the technological platform "Microsonde Ouest" (Université Bretagne Occidentale, Fr). Prior to calibration and analysis, a general scan was carried out in order to detect all chemical elements present and avoid any possible interference. Quantitative analyses for oxides and sulfides, and compositional mapping were performed with a focused beam of 1 μm diameter, at an accelerating voltage of 15 kV and 4 nA beam current.

2.2.4. BCR

The metal and metalloids distribution and reactivity in tailing samples was assessed using the modified BCR (European Community Bureau of Reference) three step sequential extraction procedure (Pérez-Cid et al., 1998). This protocol was chosen because this is a standardized protocol that easily allows comparison from one study to another one. It has already been performed successfully in previous studies (Álvarez-Valero et al., 2009; Cappuyns et al., 2007; Pascaud et al., 2013; Zhai et al., 2014). The different extraction reagents and the ratio of solid/solution for each extraction are shown in Table 1. For each sample, extraction procedure was applied on two subsamples. The solutions were filtered through a 0.45 μm cellulose acetate filters, acidified with HNO_3 and stored at 4 °C until analysis by ICP.

2.2.5. Leaching tests

The mobility of As and Pb was assess using leaching tests on crushed samples, the finely grounded materials enhancing the surface contact with the leachate and accelerating the kinetics of reaction. The chosen liquid/solid (L/S) ratio at 1/100, together with the finely grounded material, should indicate the quantity of pollutants that may be leach out, *i.e.* that may be available under environmental conditions on the long term. First experiments, carried out with deionized water at pH 6 and an ionic strength of 0.01 M ($NaNO_3$), aimed to determine the kinetics of reaction and the time for the system to reach a pseudo-equilibrium. The leachate was sub-sampled after 30 min, 1h30, 4 h then twice a day until the concentrations of As and Pb in the leachate were stable. According to the kinetics, the contact time chosen for the solubility tests was 260 h (11 days). Based on that time, following tests aimed to highlight the pH effect on the metal host phases solubility. These solubility tests were performed with a range of pH from 2 to 9 in order to simulate both Acid Mine Drainage (AMD) phenomena and pH values encountered in case of lime stabilization for instance. The pH values were adjusted and maintained adding droplets of HNO_3 or NaOH if necessary; the pH was verified twice a day. Ionic strength was fixed at 0.01 M by $NaNO_3$ to ensure that the observed trends are due to pH variations, as for the kinetic tests. Leaching tests were duplicated for 2 of the 4 samples and show a standard

Table 1
Sequential extraction protocol (BCR).

Fraction	Chemical reagents	Volume (ml)	Solid-solution ratio (g/ml)	Sonication time and power
F1: Exchangeable fraction	Acetic acid (CH_3COOH) 0.11 mol/l	20 ml	0.025	20 W for 7min
F2: Reducible fraction	Hydroxylammonium ($HONH_2 \cdot HCl$) 0.10 mol/l (reagent brought back to pH2 with nitric acid 69%)	20 ml	0.025	20 W for 7min
F3: Oxidizable fraction	Hydrogen peroxide (H_2O_2) 30%	10 ml	0.05	20 W for 2min
	Ammonium acetate ($C_2H_3O_2NH_4$) 1 mol/l (reagent brought back to pH2 with nitric acid 69%)	25 ml	0.02	20 W for 6min

deviation lower than 7%.

Eventually, the EN 12457-2 compliance test protocol, corresponding to static leaching test, was applied on crushed materials to determine the leachable content of As and Pb in tailings. In sum, 45 g of materials was mixed with 450 ml of double deionized water (18.2 $M\Omega cm^{-1}$) during 24 h at a L/S ratio of 10. Leaching solutions were filtered through a 0.45 μm cellulose acetate filters, acidified with HNO_3 and stored at 4 °C until analysis by ICP-MS. The pH was not adjusted during the leaching test.

3. Distribution of the heavy metals

Collected samples show high heterogeneity in size particles from clay to sand grain size (Table 2). Determination of the pH indicates two categories of samples: those presenting acidic pH values (pH ~ 4.6, n = 16) and those presenting neutral pH values (pH ~ 6.7, n = 11), the pH range being from 4.1 to 7.8 (Table 2).

For experimental tests, *i.e.* sequential extraction, solubility and leaching tests, eight representative samples (#1, 2, 11, 12, 13, 15, 18 & 19) were selected according to the abundance on site of the sample type based on the color/grain size/texture, their As and Pb contents and their mineralogical composition (Tables 2 and 3). Among these materials, samples # 11, 12, 15, 18 & 19 show acidic pH values on the contrary to samples # 1, 2 & 13 characterized by near-neutral pH values.

Table 2
Main physical-chemical characteristics of the waste materials (concentrations, pH and grain size distribution) and natural geochemical background at the French scale (mean, min and max values). Highlighted samples are those used for leaching tests.

Tailings	Ag	As	Cd	Fe	Mn	Pb	S	Sb	Zn	pH	<2 μm	2/20 μm	20/50 μm	50/200 μm	200/2000 μm
	mg/kg			%	mg/kg	%		mg/kg			g/kg				
1	39	688	21	1.2	464	1.4	0.5	46	2579	7.8	27	28	4	9	932
2	77	799	163	1.5	697	4.7	1.4	73	5883	6.3	132	445	243	108	72
2O	72	999	38	1.7	464	3.9	0.9	73	2849	n.d.	n.d.	n.d.	n.d.	n.d.	n.d.
3	41	849	3	1.3	310	1.8	0.5	44	541	4.4	47	27	35	40	851
4	63	700	8	2.0	619	4.0	0.8	57	1259	4.7	288	350	41	25	296
5	56	903	14	1.6	464	2.9	0.6	68	1805	6.3	48	105	77	365	405
6	58	566	57	1.5	697	3.4	0.6	46	5048	6.2	158	617	105	27	93
7	67	501	85	1.2	542	4.4	1.4	67	5654	6.8	139	352	315	135	59
8	70	698	10	1.5	387	4.5	0.4	73	1164	6.5	123	310	249	163	155
9	24	547	18	1.4	542	1.1	0.6	31	2080	7.4	48	95	161	579	117
10	61	652	17	1.9	232	3.9	0.5	42	1448	6.3	216	555	135	42	52
11	22	653	4	1.6	697	1.2	0.2	29	404	4.6	61	106	210	540	83
12	48	1014	1	1.3	l.d.	1.8	0.6	83	726	4.3	68	50	67	346	469
13	63	678	18	1.4	542	3.1	0.3	63	1533	6.9	102	232	171	314	181
14	34	399	0	1.0	l.d.	1.1	0.2	38	216	4.5	38	12	13	43	894
15	39	652	1	1.4	77	4.0	0.3	43	404	4.5	172	249	141	169	269
16	57	387	1	0.7	l.d.	2.0	0.4	51	305	4.3	47	27	7	141	778
17	59	937	3	1.0	l.d.	2.9	0.6	64	474	4.1	66	164	157	251	362
18	45	3199	3	4.1	l.d.	3.1	1.0	93	1495	4.2	84	135	125	209	447
19	115	697	134	1.6	77	6.0	1.8	75	5519	5.1	30	61	7	19	883
19O	81	916	6	2.0	l.d.	6.0	1.1	95	694	4.5	n.d.	n.d.	n.d.	n.d.	n.d.
19A	40	841	1	1.5	l.d.	1.5	0.5	52	723	n.d.	39	49	30	52	830
20	105	880	4	1.7	l.d.	6.3	1.0	92	826	5.1	153	286	256	248	57
21	111	737	92	1.6	l.d.	5.9	1.5	70	3923	5.3	142	304	302	211	41
22	35	7062	11	13.6	232	2.2	1.1	145	2798	5.1	n.d.	n.d.	n.d.	n.d.	n.d.
23	5	101	1	11.4	4257	0.3	0.1	8	124	5.0	n.d.	n.d.	n.d.	n.d.	n.d.
24	44	696	14	1.8	387	1.9	0.7	47	2316	6.1	79	138	149	354	280
Tailings *n = 24*				mg/kg				%	mg/kg		%			mg/kg	
Mean Value				57	1028		27	2.4	649		3.1	0.7	62	1955	
Min				5	101		0	0.7	77		0.3	0.1	8	124	
Max				115	7062		163	13.6	4257		6.3	1.8	145	5883	
French geochemical background[a] *n = 118*				mg/kg				g/kg	mg/kg						
Mean Value				0	21		0	24	677		49	314	2	123	
Min				0	2		0	2	5		8	50	0	2	
Max				2	224		7	62	4319		904	847	31	2904	

[a] determined according to the FOREGS database on topsoils.

Table 3
Visual description of the 24 samples and As and Pb-bearing phases identified in the waste materials according to the analytical techniques. Highlighted samples are those used for leaching tests.

Samples#	Visual description	Mineral name	Chemical formula	Identified by	Detected in sample#
1	Gray coarse sand	Mimetite	$Pb_5(AsO_4)_3Cl$	μRS, EPMA	1
2	Ochreous and blueish clay	(Hydro-) Cerussite	$PbCO_3/Pb_3(CO_3)_2(OH)_2$	XRD, μRS, EPMA	1, 2, 2O, 5, 6, 8, 9, 13, 24
2O	Ochreous clay level in 2	PbMn-oxide (cesarolite type)	$PbH_2Mn_3O_8$	SEM-EDX, EPMA	9, 13
3	Yellow sand	Anglesite	$PbSO_4$	XRD, μRS, SEM-EDX, EPMA	1,2O, 3, 4, 8, 11, 12, 14, 15, 16, 17, 18, 19, 19O, 19A, 20, 23, 24
4	Clayey				
5	Fine brown sand	Corkite		XRD, μRS, SEM-EDX	11, 19, 19O, 20, 24
6	Yellow sand	Lanarkite	$Pb_2(SO_4)O$	XRD, EPMA	1, 12
7	Gray-blueish clay	Litharge		XRD, SEM-EDX	1, 2O, 7
8	Red-ochreous clay	Beudantite	$PbFe_3(AsO_4)(SO_4)(OH)_6$	XRD, SEM-EDX, EPMA	3, 4, 5, 12, 15, 18, 19O, 19A, 22
9	Gray fine sand	Plumbojarosite	$PbFe_6(SO_4)_4(OH)_{12}$	XRD, μRS, SEM-EDX, EPMA	1, 2, 2O, 11, 12, 16, 17, 18, 19, 21
10	Red and blueish clay				
11	Ochreous coarse sand	PbFe-oxide (plumboferrite type)	$Pb_2Fe_{(11-x)}Mn_xO_{19-2x}$, $x = 1/3$	SEM-EDX, EPMA	13
12	Ochreous fine sand				
13	Ochreous sand	Hematite	Fe_2O_3	XRD, EPMA	4
14	Fine brown sand				
15	Clayey	Goethite	α-FeOOH	XRD, μRS	15, 24
16	Light yellow sand				
17	Orange coarse sand	Lepidocrocite	λ-FeOOH	XRD, μRS	11, 24
18	Coarse sand with Fe crusts				
19	Yellow sand	Galena	PbS	XRD, SEM-EDX, EPMA	1, 2, 7, 21
19O	Ochreous level in 19				
19A	Blueish level in 19	Troilite	FeS	μRS, SEM-EDX, EPMA	24
20	Ochreous clay				
21	Blueish clay	Sphalerite	ZnS	μRS, SEM-EDX, EPMA	1, 6
22	Concretions				
23	Concretions	Pyrite	FeS_2	XRD, μRS, SEM-EDX, EPMA	1, 2, 7, 19
24	Brown sand				

3.1. Chemical composition

When comparing to the natural French geochemical background, the concentrations of heavy metals from the waste materials are extremely higher, by a factor of 70–600 for Pb and by a factor of 30–50 for As (Table 2). Lead is the most abundant heavy metal with concentrations particularly high of several percent (up to 6.3%; Table 2). Waste materials are also enriched in Cd, S, Sb and Zn comparing to the natural French geochemical background.

Statistical tests were implemented to decipher whether As and Pb concentrations in the collected samples depend on pH values and/or grain size distribution. The concentration data were log transformed to homogenize their variance. The better links to grain size were shown with coarse/fine log-ratio: GRAN = log(200_2000 faction/2_20 fraction) (Fig. 2). The log-ratio eliminates the spurious correlations between fractions that sum to 100%. When plotted against grain size and pH, the data exhibit high variability (Fig. 2). To get more reliable results the robust Spearman correlation associated with Monte-Carlo exact test (10 000 samples) were used. We were not able to show any As dependence (Fig. 2 and Table 4).

On the contrary, the correlation between Pb and grain size is highly significant with an error risk less than 0.2%, indicating that the smaller are the grains, the higher the Pb concentrations are (Fig. 2 and Table 4).

3.2. Mineralogical characterization

Mineralogy of the tailings has been determined by XRD (data not shown here) but because of the analytical detection limit of this technique, the characterization was completed by μRS (Fig. 3). The morphology and quantification of the metals concentrations were obtained after SEM observations (Figs. 4 and 5) and EPMA measurements (Fig. 4). Table 3 gives the main As and Pb-host phases identified in the waste materials.

Tailing materials are composed of primary minerals: quartz, Ca–Na- and K-feldspars, clay minerals (vermiculite, chlorite, clinochlore, muscovite and illite), apatite and monazite, Ti-oxides (rutile and anatase) and carbonates (calcite, dolomite and siderite). In the region 1200-600 cm^{-1} (symmetric stretching of the CO_3^{2-} group; Sun et al., 2014), Raman spectra of dolomite and siderite exhibited a band at the same spectral position, 722 cm^{-1}, and one sharper at 1085 cm^{-1} for siderite and 1095 cm^{-1} for dolomite ascribed to the $\nu_1(CO_3)$ (Rull et al., 2004) (Fig. 3). Other characteristic bands for siderite were measured at 180 and 282 cm^{-1} (Das and Hendry, 2011; Isambert et al., 2006) and those for dolomite were found at 174 and 296 cm^{-1} (Sun et al., 2014). At higher wave number regions, bands at 1188, 1328, 1355, 1441 and 1472 cm^{-1} were also assigned to siderite and bands at 1440 cm^{-1} is also observed for dolomite.

Secondary metal host phases were determined and among them the main Pb and As host phases are summarized in Table 3 and Fig. 4a. These secondary phases correspond to minerals of the mineralization paragenesis or to newly formed phases within the waste materials resulting from supergene alteration. The most abundant phases are sulfates and carbonates such as anglesite, $PbSO_4$ (Fig. 4), lanarkite $Pb_2(SO_4)O$ (Fig. 4b), plumbojarosite $PbFe_6(SO_4)_4(OH)_{12}$ and (hydro-)cerussite $PbCO_3$ or $Pb_3(CO_3)_2(OH)_2$ (Figs. 4 and 5). Raman spectra with bands around 1000 cm^{-1} are typical of sulfate. Anglesite and plumbojarosite are well identified and they both show sharp bands indicating well-crystalline phases. Bands at 133, 441, 453, 610, 643, 980, 1060 and 1160 cm^{-1} were ascribed to anglesite (Bouchard and Smith, 2003); those measured at 141, 220, 310, 356, 437, 453, 565, 625, 1007, 1102 cm^{-1} are in agreement with previous identification of plumbojarosite (Frost et al., 2006) (Fig. 3). The large band centered at 830 cm^{-1} on the plumbojarosite Raman spectrum is ascribed to $(AsO_4)^{3-}$ stretching vibrations (Frost et al., 2007). Indeed, chemical analyses on

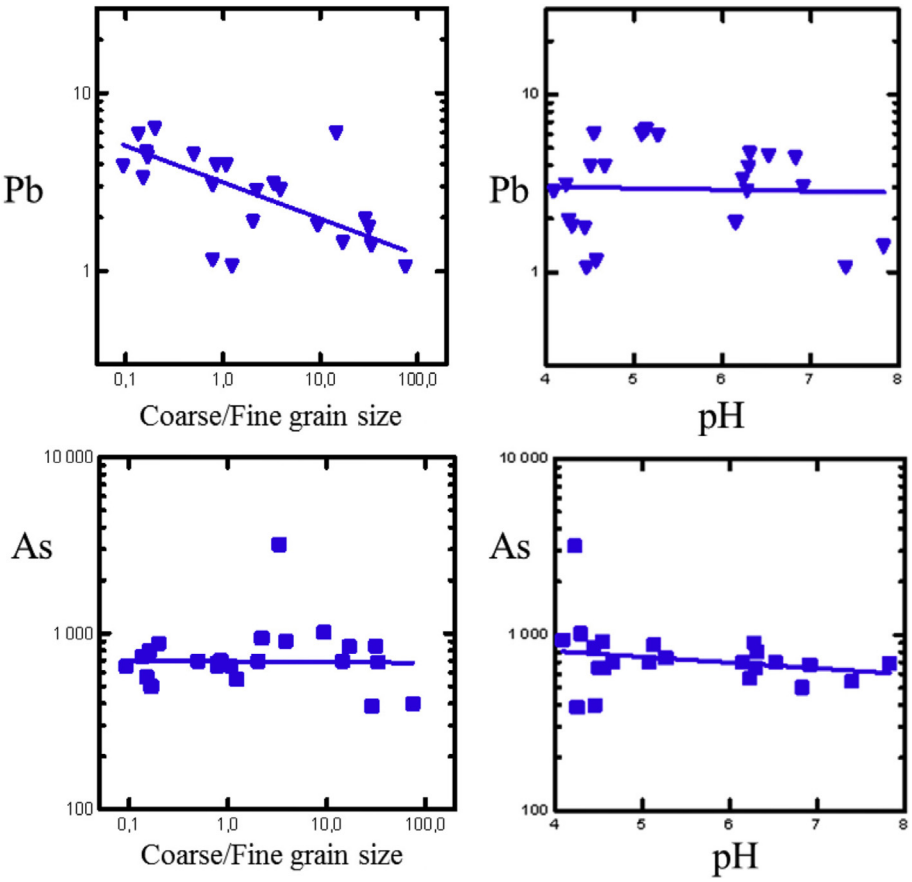

Fig. 2. Pb and As relations to grain size distribution and pH.

plumbojarosite show that As can be present up to 2.5 wt.% within this mineral by substitution with SO_4^{2-} group (Jambor, 1999) (Fig. 4a).

Anglesite is also easily recognizable from the plumbojarosite according to its massive and large size (several ten μm) when plumbojarosite forms aggregates of small size particles (few μm) (Fig. 5).

Cerussite was described as a secondary mineral in the mineralization paragenesis. Its Raman spectra show a sharp bands at 1055 cm^{-1} (very strong ν_1 vibration) and wider bands at 151, 179, 245, 668, 685, 699, 841, 1374 and 1477 cm^{-1} (Aze et al., 2006; Martens et al., 2004). A sharp and very strong band at 104 cm^{-1} is also noticed but was not reported for cerussite in other studies.

Beudantite $PbFe_3(AsO_4)(SO_4)(OH)_6$, plumboferrite-type phase $Pb_2Fe_{(11-x)}Mn_xO_{19-2x}$, $x = 1/3$ (Fig. 5) and mimetite (Figs. 4a and 5) $Pb_5(AsO_4)_3Cl$ were also identified in some samples but are less frequent. Raman spectrum obtained on mimetite shows typical bands at 313, 339, 372, 420 and 808 with a shoulder at 778 cm^{-1} (Frost et al., 2007) but the band at 970 is assigned to SO_4^{2-} ν_1 symmetric stretching mode (Frost et al., 2011). Beudantite can be distinguished from plumbojarosite according to its morphology, as it appears more massive than plumbojarosite (Fig. 5) and contains higher As concentrations (Fig. 4). As for numerous phases, Zn is present within beudantite with Zn ~2 wt.%. Plumboferrite-type phase corresponds to very fine particles, always presenting a turbostratic texture and may contain some Ag, As and also Zn (Fig. 4c) and could only be inferred by EPM and SEM-EDX analyses. Due to the texture and the thinness of the phase, Raman spectrum on this phase (not shown) mainly shows characteristic bands of epoxy resin, notably those near 1350 and 1450 cm^{-1} (CH_2 and CH_3 groups; Edwards et al., 2007; Rodriguez-Mella et al., 2014); furthermore no Raman spectrum of a plumboferrite reference material was published before. Iron (hydr-)oxides were also identified and may contain some As and/or Pb. They mainly correspond to goethite α-FeOOH, lepidocrocite γ-FeOOH and hematite Fe_2O_3 (Figs. 3 and 5). Raman spectra obtained on Pb-rich goethite show bands at 294, 398, 680, 1297 cm^{-1} (Courtin-Nomade et al., 2010) with a supplementary band noticed at 220 cm^{-1}, not reported for goethite reference material spectrum. Lepidocrocite was also identified by Raman analyses showing bands at 217, 248, 297, 345, 391, 530, 660 and 1300 cm^{-1}(Courtin-Nomade et al., 2012; Criado et al., 2013). A mixture of goethite/lepidocrocite was also frequently identified

Table 4
Usual and exact tests for the Spearman rank correlations (bilateral). The usual significance limit is $p < 5\%$ (significant value is highlighted).

	Spearman Rho	Asymptotic error risk	MC Rho value	MC error risk
Pb vs. Granulometry	−0.61	0.1%	−0.63	0.2%
Pb vs. pH	0.15	60%	0.11	60%
As vs. Granulometry	0.08	62%	0.11	61%
As vs. pH	−0.32	10%	−0.35	9%

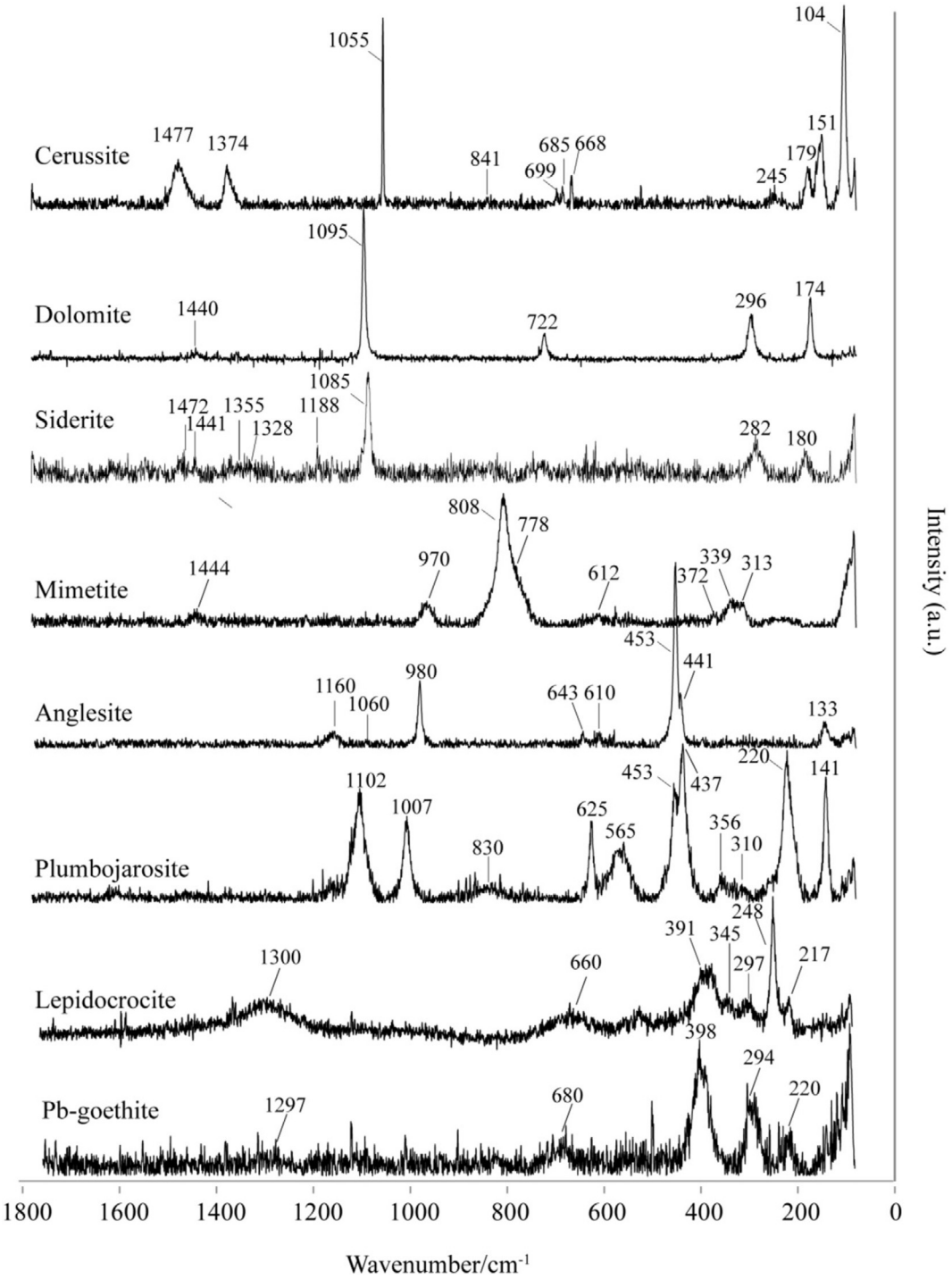

Fig. 3. Raman spectra of some heavy metal host phases identified within the tailing samples.

within the samples. As and Pb are commonly associated to goethite and lepidocrocite, this latest mineral being more widely identified within samples presenting near-neutral pH. The Pb concentrations are particularly high in these Fe-oxides, up to 7 wt%. in lepidocrocite and up to 15 wt.% in goethite, that may imply its coprecipitation and probable small size particles of these iron oxides as already suggested by Lu et al. (2011) and Rahimi et al. (2015) for lepidocrocite. Arsenic was also measured in these phases, at lower concentrations than Pb (up to 3 wt.%). Some Mn oxides have also been detected but were not formerly identified. According to SEM-EDX semi-quantitative analyses some Pb–Mn oxides show composition close to the one of cesarolite ($PbH_2Mn_3O_8$) (mean composition: Mn = 39 wt.%, Pb = 42 wt.%), when some others contain significant amount of Fe (example of typical composition Fe = 8.6 wt.%, Mn = 29.8 wt.% and Pb = 27.8 wt.%). Zinc is frequently associated to these (Fe-) (Pb-)Mn oxides (Zn ~3 wt.%). Sulfides are also still present within the tailings with the most abundant identified as arsenopyrite, galena, pyrite (sometimes arsenian pyrite), troilite and sphalerite (Table 3). They present sometimes alteration features with authigenic phases forming coating on these

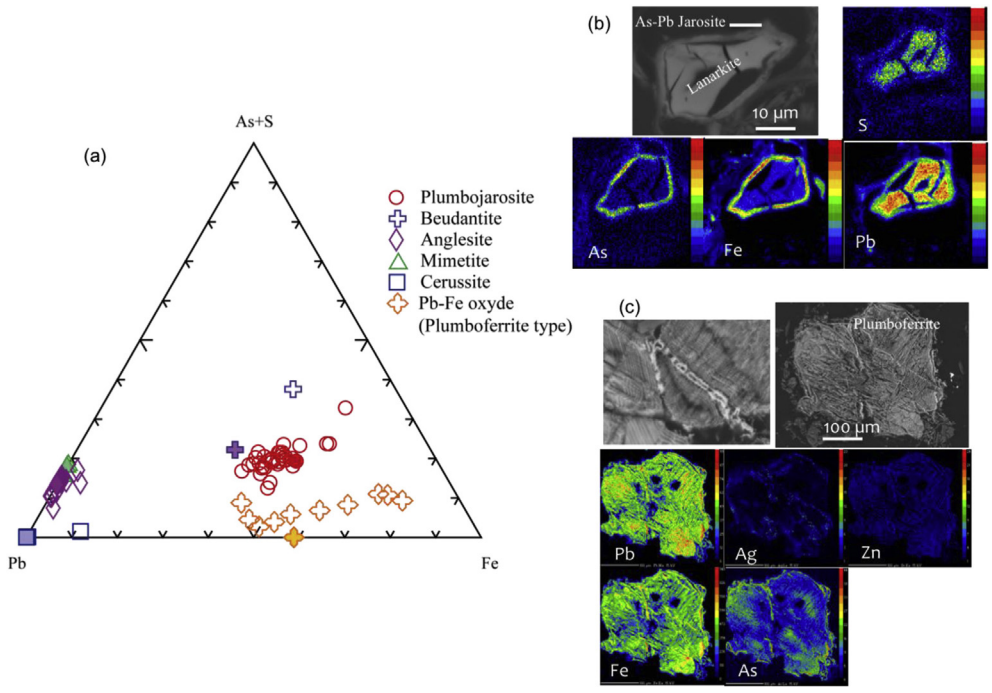

Fig. 4. (a) Ternary diagram of EPMA data of the main As and Pb host phases; SEM microphotographs and X-ray elemental map after EPMA of (b) lanarkite with a rim of As–Pb plumbojarosite and (c) Plumboferrite-type phase showing associated Ag, As and Zn.

minerals or filling the porosity (Fig. 5).

Concerning the samples chosen for the leaching experiments, samples #1, #2 and #13 have the particularity to contain (Pb-) carbonates as well as plumboferrite-type and Mn oxides. Samples #11, #12, #15 and #18 are mainly composed of sulfates (anglesite, plumbojarosite and beudantite). Iron oxides are more widespread whatever the sample but lepidocrocite is more likely present with carbonate-rich samples and goethite and hematite in the other ones. Furthermore it is noteworthy that samples with the highest content of carbonates show unaltered or few altered sulfides on the contrary to the other samples.

3.3. Chemical extraction

The proportion of As and Pb in the various host phases based on their reactivity is estimated by BCR application whose results are given in Fig. 6.

Chemical extractions results presented here only concern 4 representative samples (#1, 2, 12 and 18) which give the general trend of As and Pb behavior and distribution whatever the sample. According to the BCR results, As is predominantly found in the residual fraction (61% for #2, 72% for #12, 75%–99% for #1 and 18) while the "exchangeable" fraction represents only 0.01–2% (Fig. 6).

The oxidizable fraction represents about 20% of total As for sample #1 (18%), #2 (22%) and #12 (17%) and only 2% for #18 (Fig. 6). Finally the easily reducible fraction of As represents 10% of the sample #2 and 6% of #1 and 12 and is not detected in the sample #18 (Fig. 6). The results for #18 sample for which As-rich plumbojarosites were observed, suggest that As is incorporated into the crystal structure by substitution of sulfates by arsenate (Chen et al., 2012; Frau et al., 2009). The reducible fraction corresponds to the arsenic detected with iron and manganese oxides. The oxidizable fraction is supposed to correspond to the elements associated with organic matter (OM) but in our case we assume that the samples contain an infinitesimal amount of OM based on the total C measurement around 0.2% (data not shown). It is more likely that the arsenic oxidized fraction is related to sulfide phases by micro-inclusion in their structure. The As host phases of the residual fraction are assumed to correspond to beudantite and plumbojarosite.

In the same way, Pb in sample #18 is predominantly found in the residual fraction (85%) (Fig. 6). This coincides with the large quantities of highly stable plumbojarosite detected by XRD and SEM-EDX. This residual fraction represents 27% of sample #2, 48% of #1 and 58% of #12 (Fig. 6). The oxidizable fraction, the largest fraction for the sample #2 (45%), can be related to the presence of galena, well preserved in this sample (Fig. 6). The easily reducible fraction (4–16%) is attributed to iron oxides but can also correspond to anglesite (Fig. 6). The "exchangeable" fraction (2–16%) is the adsorbed lead and lead-related carbonates such as cerussite that is frequent in samples #1 & 2 (Fig. 6).

The behavior of Pb and As appears to be similar despite the heterogeneity of the samples. The #18 sample is however clearly distinct from the 3 others. This is linked to its mineralogy and the stability of its host phases (anglesite, beudantite and plumbojarosite). It is also possible that reactions to extract the fractions F1, F2 and F3 were not complete, meaning that some phases remain intact, and that the residual fraction is overestimated. However, the BCR results are satisfactory as the sum of the various fractions is equal to the total fraction with less than 10% error.

4. Potential impact of the heavy metals on the environment

4.1. Solubility tests

The solubility experiments were performed on the same samples analyzed by BCR. The results are presented Fig. 7. The four samples show a maximum of solubility for both As and Pb at pH = 2.

The amount of As released comparing to its total content represents 44% of As for sample #1, 45% of As for sample #2, c.a. 2–3 mg/L of As released respectively, 27% of As for sample #12

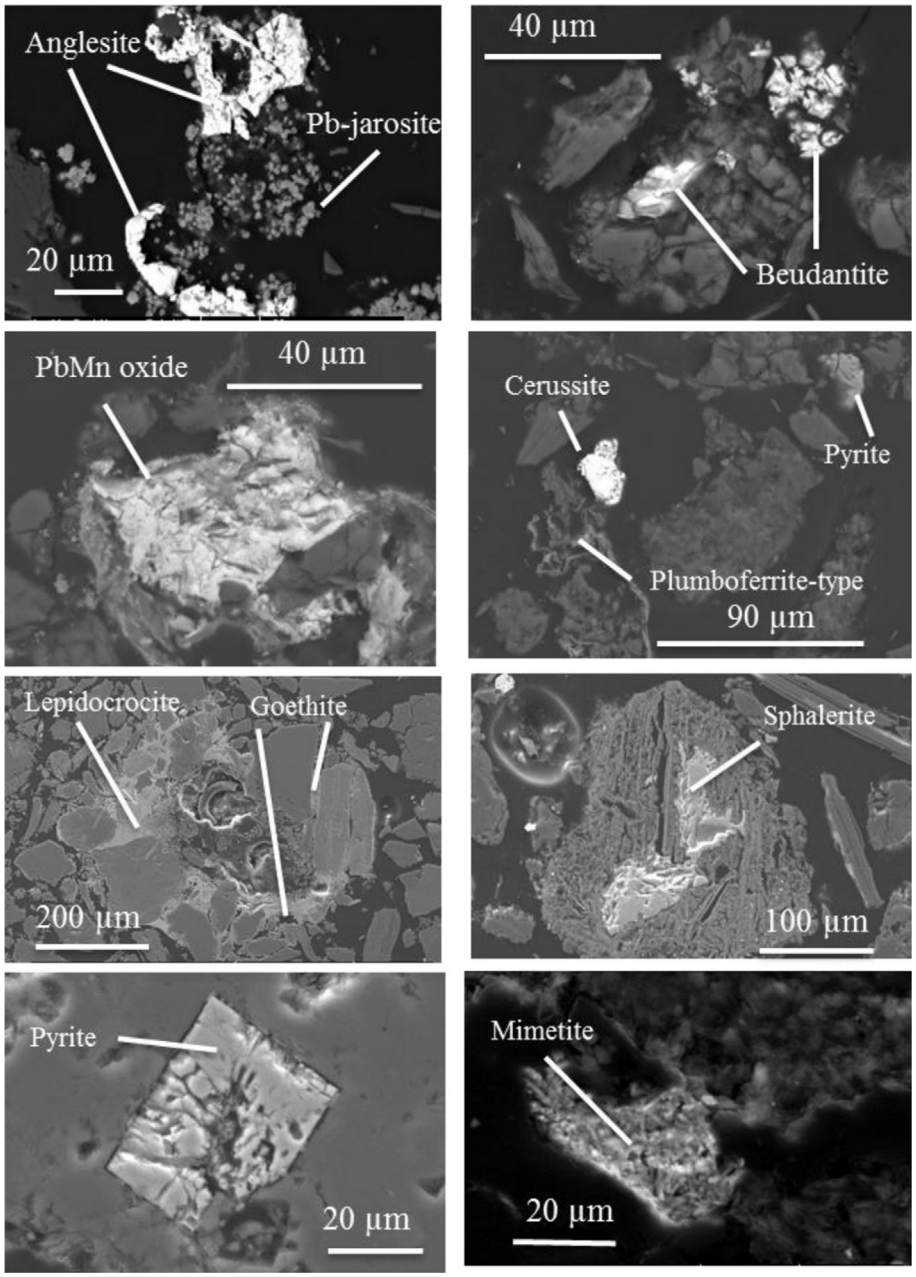

Fig. 5. SEM microphotographs of the main As and Pb host phases.

(0.8 mg/L) and 6% of As for sample #18 (0.7 mg/L) (Fig. 7).

The minimum solubility is reached at neutral pH (6 < pH < 7). Samples #2, 3 and 12 show a minimum solubility at pH 7, which correspond to 2.1 µg/L of As released from sample #1 (0.04% As_{tot}), 2.5 µg/L of As from sample #2 (0.03% As_{tot}) and 1.9 µg/L from sample # 12 (0.07% As_{tot}) (Fig. 7). The minimum solubility for

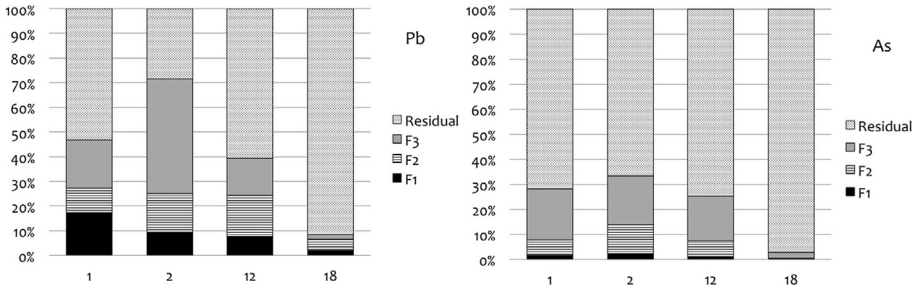

Fig. 6. Sequential extraction results according to the BCR protocol for Pb and As (F1 exchangeable fraction, F2 reducible fraction, F3 oxidizable fraction).

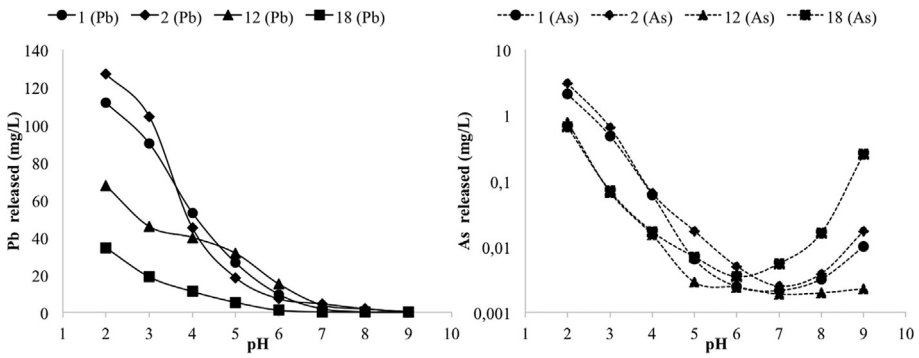

Fig. 7. Concentrations of As and Pb released in mg/L according to pH variation; solubility tests performed at pH values between 2 and 9 on four representative samples.

sample #18 is obtained at pH 6 with 3.5 μg/L of As released (0.03% As_{tot}). An increase in the released concentrations is then observed at pH 9; the highest As concentrations measured in the leachate at this value represent 0.4% of sample #1, i.e., 10 μg/L As_{tot}, 17 μg/L of As for sample #2 (0.2% As_{tot}) and 256 μg/L of As for sample #18 (2.6% As_{tot}). Only sample #12 releases 2.3 μg/L of As (0.08% As_{tot}) (Fig. 7). For basic pH values, arsenate and arsenite anions are desorbed but arsenic in sample #12 is largely present as beudantite, which should be stable under these conditions.

For Pb, at acidic pH (=2), 112 mg/L of Pb is released, corresponding to 50% of the total concentration of Pb for sample #1, 127 mg/L for sample #2 (27% of Pb_{tot}), 68 mg/L for sample #12 (37% Pb_{tot}) and 34 mg/L for sample #18 (11% Pb_{tot}) (Fig. 7). This is in agreement with the BCR results and the mineralogy; the richest samples in carbonates show the highest concentrations of Pb released at acidic pH values. The amount of Pb released decreases with increasing pH to reach a releasing capacity less than 0.1% of the total Pb content and the minimum of solubility is reached at pH = 8–9: 90 μg/L of Pb for sample #1 (0.04% Pb_{tot}), 100 μg/L of Pb for sample #2 (0.02% Pb_{tot}), 230 μg/L of Pb for sample #12 (0.01% Pb_{tot}) and only 30 μg/L of Pb for sample #18 (0.01% Pb_{tot}) (Fig. 7). These results are in good agreement with previous studies (Al-Abed et al., 2007, 2006).

Released As concentrations at pH 2 and 9 are all over the National Environmental Quality Standards for EU priority substances (NEQS), with AA-EQS (Annual Average-Environmental Quality Standards) value fixed at 4.2 μg/L, except for sample #12 (http://www.ineris.fr). They however are below that limit at *in situ* pH values. Concerning Pb concentrations measured in the leachates at pH 2, 9 or *in situ* near neutral pH, they all over exceed the AA-EQS value fixed at 1.2 μg/L (http://www.ineris.fr).

4.2. Compliance tests

In order to evaluate the immobilization of As and Pb through the waste materials, compliance tests were performed on selected samples #2, 11, 13, 15, 19. Concentrations measured after 24 h were compared to limits established by EULFD (European Landfill Directive, EUFLD, 2002). The EN 12457 limits were established for the purpose of waste disposal on landfills and to characterize waste as inert, non-hazardous and hazardous materials (Ettler et al., 2009, 2005; Nikolić et al., 2013). The results are presented in Table 5.

The metals of interest, As and Pb, show very different behavior: As is not remobilized on the contrary to Pb. Except sample #2, Pb concentrations for all the samples are over the highest limits indicating these materials cannot even be considered as hazardous wastes landfills. However Pb contents in samples #2 and 13 are the same (Table 3). It is noteworthy that the presence of carbonates does not fully explain the leachability behavior of Pb when it seems more likely to be the case for Cd. Indeed samples #2 and 13 are constituted by carbonates and they both show the highest concentrations in Cd and Zn. The main mineralogical difference between these two samples is the presence of more abundant Pb–Mn oxides (cesarolite-type) and Pb–Fe oxides (plumboferrite-type) within sample #13 when sulfates dominate the mineralogy of sample #2. Concerning the other samples, the main mineralogical difference with samples #2 and 13 is that Pb is associated to abundant Fe oxides. The highest Pb concentrations are measured for samples with the highest content of Fe oxides (#11 and 15). These results can be explained regarding the reported solubility constants for anglesite (Ksp = $10^{-7.7}$) and plumbojarosite (Ksp = $10^{-11.42}$–$10^{-28.4}$) (Eary, 1999; Forray et al., 2010; Gaboreau and Vieillard, 2004), appearing quite stable, cerussite Ksp = $10^{-13.13}$, also ensuring good immobilization of Pb but with a more pH dependent behavior, and goethite Ksp = $10^{-0.5}$ (Eary, 1999), the less stable mineral among the other host phases. However all the plumbojarosites analyzed at that site contain As that may increase its solubility (Frau et al., 2009).

The compliance tests are performed with deionized water at pH around 5.5, which is a value for which the minimum of solubility of As is reached when it is still not the case for Pb (Fig. 7). At the end of the tests the pH remains quite stable for samples with carbonates (pH ~5 for #2 & 13) but lower values are measured (4 < pH < 4.3) for the other samples. However this pH value well represents the pH of meteoric water and thus gives a good overview of the potential mobilization of heavy metals from that wastes.

5. Conclusion

Under supergene conditions, sulfides are oxidized and associated metals are remobilized as well as production of acidity. Galena, the dominant sulfide at this studied site, is directly oxidized in

Table 5
Compliance test results of some tailing samples according to the EU waste acceptance criteria. Underlined samples exceed the upper limit value.

(Mg/kg)	2	11	13	15	19	Limit value for inert waste landfills	Limit value for non-hazardous waste landfills	Limit value for hazardous waste landfills
As	0.01	0.01	0.1	0.02	0.03	0.5	2	25
Pb	38	123	215	185	100	0.5	10	50

anglesite which then will be dissolved and will release Pb^{2+} and SO_4^{2-} ions (Batonneau et al., 2000). Pyrite and carbonate such as siderite, when oxidized, will liberate directly Fe and SO_4^{2-} in solution. Thus secondary phases may form if they are in a supersaturated state. Among the predominant phases, plumbojarosite and beudantite are more stable and result in minimal release of As and Pb. Lead is also present as Pb–Mn oxides or as Fe–Mn phases such as plumboferrite-like phases, the latest appearing unstable under low acidic pH (5.5). The adsorbed metal elements, particularly on Fe and Mn oxides are the most mobile as already observed in some previous studies (Audry et al., 2006; Lee et al., 2005). Carbonated phases are very unstable under acidic conditions but anglesite also tends to be dissolved in acidic conditions (Bigham et al., 2013). However, in this study, the presence of these abundant carbonates allows neutralizing acidity generated by sulfides oxidation but they do not prevent the heavy metals release from the waste material toward the aqueous compartment. Indeed, leaching tests show that As and especially Pb are mobile, with concentrations in the leachates often exceeding the AA-EQS.

At the Auzelles district, tailing materials affect the local river and its ecosystem by solid transport but also by dissolved metals inputs. The knowledge of the heavy metals mineralogy and their susceptibility to weathering should help in sustainable waste management and in the remediation choices between stakeholders and policy makers.

Acknowledgments

This study is part of the MetMines program for which financial support was provided by the French Water Agency – Agence de l'Eau Loire Bretagne (AELB, France) and the European regional funding (FEDER – PRESAGE 35624) via the Plan Loire Grandeur Nature/Etablissement Public Loire (EPL). The study is a part of the Observation Network of the Loire River Basin Sediments (OSLA/ZAL). We would like to thank Patrice Fondanèche for the time he spent with Thomas during the AAS-GF analyses, Elie Dhivert, Marc Desmet, Anthony Foucher and Lauren Valverde for their help with samples collection.

References

Al-Abed, S.R., Hageman, P.L., Jegadeesan, G., Madhavan, N., Allen, D., 2006. Comparative evaluation of short-term leach tests for heavy metal release from mineral processing waste. Sci. Total Environ. 364, 14–23. http://dx.doi.org/10.1016/j.scitotenv.2005.10.021.

Al-Abed, S.R., Jegadeesan, G., Purandare, J., Allen, D., 2007. Arsenic release from iron rich mineral processing waste: influence of pH and redox potential. Chemosphere 66, 775–782. http://dx.doi.org/10.1016/j.chemosphere.2006.07.045.

Álvarez-Valero, A.M., Sáez, R., Pérez-López, R., Delgado, J., Nieto, J.M., 2009. Evaluation of heavy metal bio-availability from Almagrera pyrite-rich tailings dam (Iberian Pyrite Belt, SW Spain) based on a sequential extraction procedure. J. Geochem. Explor 102, 87–94. http://dx.doi.org/10.1016/j.gexplo.2009.02.005.

Arenas-Lago, D., Lago-Vila, M., Rodríguez-Seijo, A., Andrade, M.L., Vega, F.A., 2014. Risk of metal mobility in soils from a Pb/Zn depleted mine (Lugo, Spain). Environ. Earth Sci. 72, 2541–2556. http://dx.doi.org/10.1007/s12665-014-3161-5.

Asta, M.P., Cama, J., Martínez, M., Giménez, J., 2009. Arsenic removal by goethite and jarosite in acidic conditions and its environmental implications. J. Hazard. Mater 171, 965–972. http://dx.doi.org/10.1016/j.jhazmat.2009.06.097.

Audry, S., Blanc, G., Schäfer, J., 2006. Solid state partitioning of trace metals in suspended particulate matter from a river system affected by smelting-waste drainage. Sci. Total Environ. 363, 216–236. http://dx.doi.org/10.1016/j.scitotenv.2005.05.035.

Aze, S., Vallet, J.-M., Baronnet, A., Grauby, O., 2006. The fading of red lead pigment in wall paintings: tracking the physico-chemical transformations by means of complementary micro-analysis techniques. Eur. J. Mineral. 18, 835–843. http://dx.doi.org/10.1127/0935-1221/2006/0018-0835.

Batonneau, Y., Bremard, C., Laureyns, J., Merlin, J.C., 2000. Microscopic and Imaging Raman Scattering Study of PbS and its Photo-oxidation Product, vol. 31, pp. 1113–1119.

Bossy, A., Grosbois, C., Beauchemin, S., Courtin-Nomade, A., Hendershot, W., Bril, H., 2010. Alteration of As-bearing phases in a small watershed located on a high grade arsenic-geochemical anomaly (French Massif Central). Appl. Geochem. 25, 1889–1901.

Bouchard, M., Smith, D.C., 2003. Catalogue of 45 reference Raman spectra of minerals concerning research in art history or archaeology, especially on corroded metals and coloured glass. Spectrochim. Acta – Part A Mol. Biomol. Spectrosc. 59, 2247–2266. http://dx.doi.org/10.1016/S1386-1425(03)00069-6.

Cappuyns, V., Swennen, R., Niclaes, M., 2007. Application of the BCR sequential extraction scheme to dredged pond sediments contaminated by Pb-Zn mining: a combined geochemical and mineralogical approach. J. Geochem. Explor 93, 78–90. http://dx.doi.org/10.1016/j.gexplo.2006.10.001.

Chen, L., Li, J.-W., Rye, R.O., Benzel, W.M., Lowers, H.A., He, M.-Z., 2012. Mineralogical, chemical, and crystallographic properties of supergene jarosite-group minerals from the Xitieshan Pb-Zn sulfide deposit, northern Tibetan Plateau, China. Mineral. Petrol. 107, 487–499. http://dx.doi.org/10.1007/s00710-012-0258-y.

Courtin-Nomade, A., Bril, H., Neel, C., Lenain, J.-F., 2003. Arsenic in iron cements developed within tailings of a former metalliferous mine—Enguialès, Aveyron, France. Appl. Geochem. 18, 395–408. http://dx.doi.org/10.1016/S0883-2927(02)00098-7.

Courtin-Nomade, A., Grosbois, C., Marcus, M.A., Fakra, S.C., Beny, J.M., Foster, A.L., 2009. The weathering of a sulfide orebody: speciation and fate of some potential contaminants. Can. Mineral. 47, 493–508.

Courtin-Nomade, A., Bril, H., Bény, J.M., Kunz, M., Tamura, N., 2010. Sulfide oxidation observed using micro-Raman spectroscopy and micro-X-ray diffraction: the importance of water/rock ratios and pH conditions. Am. Mineral. 95, 582–591.

Courtin-Nomade, A., Rakotoarisoa, O., Bril, H., Grybos, M., Forestier, L., Foucher, F., Kunz, M., 2012. Weathering of Sb-rich mining and smelting residues: insight in solid speciation and soil bacteria toxicity. Chem. Erde – Geochem. 72, 29–39. http://dx.doi.org/10.1016/j.chemer.2012.02.004.

Craw, D., Koons, P.O., Chappell, D.A., 2002. Arsenic distribution during formation and capping of an oxidised sulphidic minesoil, Macraes mine, New Zealand. J. Geochem. Explor 76, 13–29. http://dx.doi.org/10.1016/S0375-6742(02)00202-9.

Criado, M., Martínez-Ramirez, S., Fajardo, S., Gõmez, P.P., Bastidas, J.M., 2013. Corrosion rate and corrosion product characterisation using Raman spectroscopy for steel embedded in chloride polluted fly ash mortar. Mater. Corros. 64, 372–380. http://dx.doi.org/10.1002/maco.201206714.

Das, S., Hendry, M.J., 2011. Application of Raman spectroscopy to identify iron minerals commonly found in mine wastes. Chem. Geol. 290, 101–108. http://dx.doi.org/10.1016/j.chemgeo.2011.09.001.

Donahue, R., Hendry, M.J., 2003. Geochemistry of arsenic in uranium mine mill tailings, Saskatchewan, Canada. Appl. Geochem. 18, 1733–1750. http://dx.doi.org/10.1016/S0883-2927(03)00106-9.

Drahota, P., Rohovec, J., Filippi, M., Mihaljevič, M., Rychlovský, P., Červený, V., Pertold, Z., 2009. Mineralogical and geochemical controls of arsenic speciation and mobility under different redox conditions in soil, sediment and water at the Mokrsko-West gold deposit. Czech Repub. Sci. Total Environ. 407, 3372–3384. http://dx.doi.org/10.1016/j.scitotenv.2009.01.009.

Eary, L.E., 1999. Geochemical and equilibrium trends in mine pit lakes. Appl. Geochem. 14, 963–987. http://dx.doi.org/10.1016/S0883-2927(99)00049-9.

Edwards, H.G.M., Beale, E., Garrington, N.C., Alia, J.–M., 2007. FT-Raman spectroscopy of pigments on a Hindu statue, Kali Walking on Siva. J. Raman Spectrosc. 38, 316–322. http://dx.doi.org/10.1002/jrs.1645.

Ettler, V., Mihaljevič, M., Šebek, O., Strnad, L., 2005. Leaching of APC residues from secondary Pb metallurgy using single extraction tests: the mineralogical and the geochemical approach. J. Hazard. Mater. 121, 149–157. http://dx.doi.org/10.1016/j.jhazmat.2005.02.001.

Ettler, V., Johan, Z., Kříbek, B., Šebek, O., Mihaljevič, M., 2009. Mineralogy and environmental stability of slags from the Tsumeb smelter, Namibia. Appl. Geochem. 24, 1–15. http://dx.doi.org/10.1016/j.apgeochem.2008.10.003.

Forray, F.L., Smith, a. M.L., Drouet, C., Navrotsky, a., Wright, K., Hudson-Edwards, K. a., Dubbin, W.E., 2010. Synthesis, characterization and thermochemistry of a Pb-jarosite. Geochim. Cosmochim. Acta 74, 215–224. http://dx.doi.org/10.1016/j.gca.2009.09.033.

Frau, F., Ardau, C., Fanfani, L., 2009. Environmental geochemistry and mineralogy of lead at the old mine area of Baccu Locci (south-east Sardinia, Italy). J. Geochem. Explor. 100, 105–115. http://dx.doi.org/10.1016/j.gexplo.2008.01.005.

Frost, R.L., Wills, R.-A., Weier, M.L., Martens, W., Mills, S., 2006. A Raman spectroscopic study of selected natural jarosites. Spectrochim. Acta. A. Mol. Biomol. Spectrosc. 63, 1–8. http://dx.doi.org/10.1016/j.saa.2005.03.034.

Frost, R.L., Bouzaid, J.M., Palmer, S., 2007. The structure of mimetite, arsenian pyromorphite and hedyphane – a Raman spectroscopic study. Polyhedron 26, 2964–2970. http://dx.doi.org/10.1016/j.poly.2007.01.038.

Frost, R.L., Palmer, S.J., Xi, Y., 2011. Raman spectroscopy of the multi anion mineral arsentsumebite Pb2Cu(AsO4)(SO4)(OH) and in comparison with tsumebite Pb2Cu(PO4)(SO4)(OH). Spectrochim. Acta. A. Mol. Biomol. Spectrosc. 83, 449–452. http://dx.doi.org/10.1016/j.saa.2011.08.063.

Gaboreau, S., Vieillard, P., 2004. Prediction of Gibbs free energies of formation of minerals of the alunite supergroup. Geochim. Cosmochim. Acta 68, 3307–3316. http://dx.doi.org/10.1016/j.gca.2003.10.040.

Gault, A.G., Cooke, D.R., Townsend, A.T., Charnock, J.M., Polya, D.A., 2005. Mechanisms of arsenic attenuation in acid mine drainage from Mount Bischoff, western Tasmania. Sci. Total Environ. 345, 219–228. http://dx.doi.org/10.1016/j.scitotenv.2004.10.030.

González-Corrochano, B., Esbrí, J.M., Alonso-Azcárate, J., Martínez-Coronado, a., Jurado, V., Higueras, P., 2014. Environ.mental geochemistry of a highly polluted

area: the La Union Pb-Zn mine (Castilla-La Mancha region, Spain). J. Geochem. Explor. 144, 345–354. http://dx.doi.org/10.1016/j.gexplo.2014.02.014.
Grosbois, C., Courtin-Nomade, A., Martin, F., Bril, H., 2007. Transportation and evolution of trace element bearing phases in stream sediments in a mining – influenced basin (Upper Isle River, France). Appl. Geochem. 22, 2362–2374.
Grosbois, C., Schäfer, J., Bril, H., Blanc, G., Bossy, a, 2009. Deconvolution of trace element (As, Cr, Mo, Th, U) sources and pathways to surface waters of a gold mining-influenced watershed. Sci. Total Environ. 407, 2063–2076. http://dx.doi.org/10.1016/j.scitotenv.2008.11.012.
Grosbois, C., Meybeck, M., Lestel, L., Lefèvre, I., Moatar, F., 2012. Severe and contrasted polymetallic contamination patterns (1900-2009) in the Loire River sediments (France). Sci. Total Environ. 435–436, 290–305. http://dx.doi.org/10.1016/j.scitotenv.2012.06.056.
Hayes, S.M., Webb, S.M., Bargar, J.R., O'Day, P.A., Maier, R.M., Chorover, J., 2012. Geochemical weathering increases lead bioaccessibility in semi-arid mine tailings. Environ. Sci. Technol. 46, 5834–5841. http://dx.doi.org/10.1021/es300603s.
Isambert, A., De Resseguier, T., Gloter, A., Reynard, B., Guyot, F., Valet, J.-P., 2006. Magnetite-like nanocrystals formed by laser-driven shocks in siderite. Earth Planet. Sci. Lett. 243, 820–827. http://dx.doi.org/10.1016/j.epsl.2006.01.060.
Jambor, J.L., 1999. Nomenclature of the alunite supergroup. Can. Mineral. 37, 1323–1341. http://dx.doi.org/10.2113/gscanmin.38.5.1298.
Kocourková, E., Sracek, O., Houzar, S., Cempírek, J., Losos, Z., Filip, J., Hršelová, P., 2011. Geochemical and mineralogical control on the mobility of arsenic in a waste rock pile at Dlouhá Ves, Czech Republic. J. Geochem. Explor 110, 61–73. http://dx.doi.org/10.1016/j.gexplo.2011.02.009.
Lee, P.K., Kang, M.J., Choi, S.H., Touray, J.C., 2005. Sulfide oxidation and the natural attenuation of arsenic and trace metals in the waste rocks of the abandoned Seobo tungsten mine, Korea. Appl. Geochem. 20, 1687–1703. http://dx.doi.org/10.1016/j.apgeochem.2005.04.017.
Lu, P., Nuhfer, N.T., Kelly, S., Li, Q., Konishi, H., Elswick, E., Zhu, C., 2011. Lead coprecipitation with iron oxyhydroxide nano-particles. Geochim. Cosmochim. Acta 75, 4547–4561. http://dx.doi.org/10.1016/j.gca.2011.05.035.
Macdonald, R.W., Barrie, L.A., Bidleman, T.F., Diamond, M.L., Gregor, D.J., Semkin, R.G., Strachan, W.M.J., Li, Y.F., Wania, F., Alaee, M., Alexeeva, L.B., Backus, S.M., Bailey, R., Bewers, J.M., Gobeil, C., Halsall, C.J., Harner, T., Hoff, J.T., Jantunen, L.M.M., Lockhart, W.L., Mackay, D., Muir, D.C.G., Pudykiewicz, J., Reimer, K.J., Smith, J.N., Stern, G., Schroeder, W.H., Wagemann, R., Yunker, M.B., 2000. Contaminants in the Canadian Arctic: 5 years of progress in understanding sources, occurrence and pathways. Sci. Total Environ. 254, 93–234. http://dx.doi.org/10.1016/S0048-9697(00)00434-4.
Martens, W.N., Rintoul, L., Kloprogge, J.T., Frost, R.L., 2004. Single crystal raman spectroscopy of cerussite. Am. Mineral. 89, 352–358.
Miler, M., Gosar, M., 2012. Characteristics and potential environmental influences of mine waste in the area of the closed Mežica Pb–Zn mine (Slovenia). J. Geochem. Explor 112, 152–160. http://dx.doi.org/10.1016/j.gexplo.2011.08.012.
Moriarty, M.M., Lai, V.W.-M., Koch, I., Cui, L., Combs, C., Krupp, E.M., Feldmann, J., Cullen, W.R., Reimer, K.J., 2014. Speciation and toxicity of arsenic in mining-affected lake sediments in the Quinsam watershed. Br. Columbia. Sci. Total Environ. 466–467, 90–99. http://dx.doi.org/10.1016/j.scitotenv.2013.07.005.
Murray, J., Kirschbaum, A., Dold, B., Mendes Guimaraes, E., Pannunzio Miner, E., 2014. Jarosite versus Soluble Iron-Sulfate Formation and Their Role in Acid Mine Drainage Formation at the Pan de Azúcar Mine Tailings (Zn-Pb-Ag), NW Argentina. Minerals 4, 477–502. http://dx.doi.org/10.3390/min4020477.
Néel, C., Bril, H., Courtin-Nomade, A., Dutreuil, J.P., 2003. Factors affecting natural development of soil on 35-year-old sulphide-rich mine tailings. Geoderma 111, 1–20.
Nikolić, I., Đurović, D., Blečić, D., Zejak, R., Karanović, L., Mitsche, S., Radmilović, V.R., 2013. Geopolymerization of coal fly ash in the presence of electric arc furnace dust. Min. Eng. 49, 24–32. http://dx.doi.org/10.1016/j.mineng.2013.04.007.
Pascaud, G., Leveque, T., Soubrand, M., Boussen, S., Joussein, E., Dumat, C., 2013. Environmental and health risk assessment of Pb, Zn, as and Sb in soccer field soils and sediments from mine tailings: solid speciation and bioaccessibility. Environ. Sci. Pollut. Res. 21, 4254–4264. http://dx.doi.org/10.1007/s11356-013-2297-2.
Pérez-Cid, B., Lavilla, I., Bendicho, C., 1998. Speeding up of a three-stage sequential extraction method for metal speciation using focused ultrasound. Anal. Chim. Acta 360, 35–41. http://dx.doi.org/10.1016/S0003-2670(97)00718-6.
Rahimi, S., Moattari, R.M., Rajabi, L., Derakhshan, A.A., Keyhani, M., 2015. Iron oxide/hydroxide (α,γ-FeOOH) nanoparticles as high potential adsorbents for lead removal from polluted aquatic media. J. Ind. Eng. Chem. 23, 33–43. http://dx.doi.org/10.1016/j.jiec.2014.07.039.
Rodriguez-Mella, Y., López-Morán, T., López-Quintela, M.A., Lazzari, M., 2014. Durability of an industrial epoxy vinyl ester resin used for the fabrication of a contemporary art sculpture. Polym. Degrad. Stab. 107, 277–284. http://dx.doi.org/10.1016/j.polymdegradstab.2014.02.008.
Romero, F.M., Prol-Ledesma, R.M., Canet, C., Alvares, L.N., Pérez-Vázquez, R., 2010. Acid drainage at the inactive Santa Lucia mine, western Cuba: natural attenuation of arsenic, barium and lead, and geochemical behavior of rare earth elements. Appl. Geochem. 25, 716–727. http://dx.doi.org/10.1016/j.apgeochem.2010.02.004.
Roussel, C., Néel, C., Bril, H., 2000. Minerals controlling arsenic and lead solubility in an abandoned gold mine tailings. Sci. Total Environ. 263, 209–219. http://dx.doi.org/10.1016/S0048-9697(00)00707-5.
Rull, F., Martinez-Frias, J., Sansano, a., Medina, J., Edwards, H.G.M., 2004. Comparative micro-Raman study of the Nakhla and Vaca Muerta meteorites. J. Raman Spectrosc. 35, 497–503. http://dx.doi.org/10.1002/jrs.1177.
Savage, K.S., Tingle, T.N., O'Day, P. a., Waychunas, G. a., Bird, D.K., 2000. Arsenic speciation in pyrite and secondary weathering phases, mother Lode gold district, Tuolumne County, California. Appl. Geochem. 15, 1219–1244. http://dx.doi.org/10.1016/S0883-2927(99)00115-8.
Sejkora, J., Škovíra, J., Čejka, J., Plášil, J., 2012. Cu-rich members of the beudantite-segnitite series from the Krupka ore district, the Krušné hory Mountains, Czech Republic. J. Geosci. 54, 355–371. http://dx.doi.org/10.3190/jgeosci.055.
Shuhaimi-Othman, M., Nadzifah, Y., Nur-Amalina, R., Umirah, N.S., 2012. Deriving freshwater quality criteria for iron, lead, nickel, and zinc for protection of aquatic life in Malaysia. ScientificWorldJournal 2012, 861576. http://dx.doi.org/10.1100/2012/861576.
Smuda, J., Dold, B., Friese, K., Morgenstern, P., Glaesser, W., 2007. Mineralogical and geochemical study of element mobility at the sulfide-rich Excelsior waste rock dump from the polymetallic Zn-Pb-(Ag-Bi-Cu) deposit, Cerro de Pasco, Peru. J. Geochem. Explor. 92, 97–110. http://dx.doi.org/10.1016/j.gexplo.2006.08.001.
Sun, J., Wu, Z., Cheng, H., Zhang, Z., Frost, R.L., 2014. A Raman spectroscopic comparison of calcite and dolomite. Spectrochim. Acta. A. Mol. Biomol. Spectrosc. 117, 158–162. http://dx.doi.org/10.1016/j.saa.2013.08.014.
Wetzel, M.A., Wahrendorf, D.-S., von der Ohe, P.C., 2013. Sediment pollution in the Elbe estuary and its potential toxicity at different trophic levels. Sci. Total Environ. 449, 199–207. http://dx.doi.org/10.1016/j.scitotenv.2013.01.016.
Yang, J.S., Lee, J.Y., Baek, K., Kwon, T.S., Choi, J., 2009. Extraction behavior of As, Pb, and Zn from mine tailings with acid and base solutions. J. Hazard. Mater 171, 443–451. http://dx.doi.org/10.1016/j.jhazmat.2009.06.021.
Zhai, Y., Liu, X., Chen, H., Xu, B., Zhu, L., Li, C., Zeng, G., 2014. Source identification and potential ecological risk assessment of heavy metals in PM2.5 from Changsha. Sci. Total Environ. 493, 109–115. http://dx.doi.org/10.1016/j.scitotenv.2014.05.106.